Marangoni and temperature dependent wetting phenomena in picoliter size solder droplet deposition

M. Dietzel, D. Poulikakos

Laboratory of Thermodynamics in Emerging Technologies
Institute of Energy Technology, Department of Mechanical and Process Engineering
Swiss Federal Institute of Technology
ETH Center, 8092 Zurich, Switzerland

The effect of the temperature dependence of surface tension (Marangoni effect) and of the wetting phenomenon on the spreading and final post-solidification shape of a molten Sn63Pb solder droplet deposited on a flat substrate is investigated. A Lagrangian finite element formulation of the complete axisymmetric Navier-Stokes equations is utilized for the description of the droplet behavior. Linear temperature dependence of the surface tension and a wetting model based on a balance of the interfacial tensions at the contact line are assumed. The droplet superheat is varied in steps of 100K from 200ºC to 500ºC, whereby the Marangoni number Ma alters from –9 to –49. The initial Weber number We_0 and initial Prandtl number Pr_0 are for all cases O(1) and O(10^{-2}), respectively. The initial impact velocity and the droplet diameter remain unchanged in all cases examined at 1.5 m/s and 80 microns. A novel adaptive mesh refinement is employed and the results are compared to those obtained earlier with a fixed grid size and the Navier-Slip condition applied at the contact line.

1 Introduction

The deposition of droplets on a flat surface has been of scientific interest for decades through their widespread occurrence in daily life and technical applications. Modern fabrication techniques demand temporal and spatial predictions in droplet motion and shape with high expectations in the accuracy, especially for small system sizes in the manufacturing of MEMS and microelectronics. The deposition of molten picoliter size solder droplets with diameter O(100μm) upon a flat copper substrate is examined in this context, thereby focusing on the effects of a temperature dependence of surface tension (temperature-induced Marangoni effect) and wetting.

Earlier investigations have shown that the impact velocity and surface tension are important parameters determining the fluid mechanical behavior of the droplet upon impact within the parametric domain of solder jetting processes [1]. Wetting effects were considered as being negligible, at least in the initial stage of the droplet impact where inertia forces dominate. It was shown that the contact line is arrested by freezing before wetting effects gain the dominance within the droplet deposition process. However, [2] showed recently that droplet spreading might be arrested by surface tension forces instead of freezing

if the Marangoni effect is considered. Moreover, the pure solid copper substrate used in this study possesses a high surface energy compared to the surface energy of the liquid solder (1710 mJ/m^2 versus 499 mJ/m^2). This makes an increased wetting very likely due to the high gradient in thermodynamic potential. The low impact velocities of O (1m/s) ensure that no splashing occurs.

The movement of the contact line has been subject of intense research since the beginning of the seventies. A standout-paper is the one of [3], which stated a stress singularity at the contact line if a no-slip condition is applied. The abandonment of the no-slip condition at the contact line imposes locally an additional degree of freedom which has to be constrained by an empirical model. This is rooted in the dominance of discrete, mesoscopic effects at the contact line, which cannot be captured a priori in a continuous hydrodynamic model. In fact, simulations on the molecular level showed useful wetting behaviors [4], but the system size is usually very limited and the computations are expensive. The most prominent contact line model is the Navier-slip condition [5], which relates the slip velocity at the contact line linearly to the local fluid stresses. Another approach is the Hoffman-Tanner-Voinov law, which defines the contact line velocity to the contact angle hysteresis [6]. [7] explicitly specified the curvature of the free surface at the contact line as a function of the dynamic contact angle. The advancing and receding contact angle was determined experimentally and used as an input value for the numerical model. More physical attempts to find an expression for the contact line velocity are often based on the gradient of thermodynamic potential as the driving force of wetting [8]. This will be also the approach in this study.

The numerical description herein is based on the Lagrangian formulation of the axisymmetric, unsteady Navier-Stokes equations, and the energy equation, with a Galerkin finite element discretization and a deforming triangulation mesh. The implementation employed extends the methodology of [9] to account for the temperature dependence of the surface tension and to include a wetting force at the contact line. Moreover, the formerly used commercial meshing tool was replaced by public-domain software.

2 Governing equations and solution procedure

2.1 Basic set of equations

The mathematical description of the problem in a dimensionless Lagrangian form of the Navier Stokes equations is:

$$D_\tau P + \frac{\nabla \cdot \vec{V}}{M^2} = 0 \qquad \text{Continuity} \tag{1}$$

$$D_\tau \vec{V} - \nabla \cdot \underline{\underline{\bar{T}}} + \frac{\vec{n}_Z}{Fr} = 0 \qquad \text{Momentum} \tag{2}$$

$$D_\tau \Theta_i - \frac{2}{Pe_i} \nabla^2 \Theta_i = 0 \qquad \text{Energy, } i = 1 \text{ - Droplet, } i = 2 \text{ - Substrate} \tag{3}$$

The dimensionless coordinates, velocities, time, pressure and temperature read:

$$R = \frac{r}{d_0},\ Z = \frac{z}{d_0},\ U = \frac{u}{v_0},\ V = \frac{v}{v_0},\ \tau = \frac{t}{d_0 / v_0},\ P = \frac{p - p_{amb}}{\rho v_0^2},\ \Theta_i = \frac{T_i - T_{2,0}}{T_{1,0} - T_{2,0}} \tag{4}$$

The dimensionless stress tensor and its components $\overline{\sigma_{ij}}$ are defined as follows:

$$\overline{\underline{T}} = \begin{bmatrix} \overline{\sigma_{RR}} & \overline{\sigma_{RZ}} & 0 \\ \overline{\sigma_{RZ}} & \overline{\sigma_{ZZ}} & 0 \\ 0 & 0 & \overline{\sigma_{\theta\theta}} \end{bmatrix} \qquad \begin{aligned} \bar{\sigma}_{RR} &= -P + \frac{2}{Re}\partial_R U\,, \quad \bar{\sigma}_{ZZ} = -P + \frac{2}{Re}\partial_Z V \\ \bar{\sigma}_{\theta\theta} &= -P + \frac{2}{Re}\frac{U}{R}, \qquad \bar{\sigma}_{RZ} = \frac{1}{Re}\left(\partial_Z U + \partial_R V\right) \end{aligned} \tag{5}$$

The initial Reynolds, Froude, Mach, Weber and Peclet number are defined as:

$$Re_0 = \frac{\rho v_0 d_0}{\mu_0}\,, \quad Fr = \frac{v_0^2}{d_0 g}\,, \quad M = \frac{v_0}{c}\,, \quad We_0 = \frac{\rho d_0 v_0^2}{\gamma_0}\,, \quad Pe_i = Re_{0i} \cdot Pr_{0i} = \frac{d_0 v_0}{\alpha_i} \tag{6}$$

where α_i represents the thermal diffusivities of the different regions (i = 1 droplet, i =2 substrate). At the initial stage, the droplet is spherical and moves downwards with a dimensionless velocity of -1. In this stage, the temperature- and pressure-fields are uniform ($\Theta_{1,0}$ = 1; $\Theta_{2,0}$ = 0; P_0 = 4/We_0). The free surface of the droplet and the substrate are considered to be adiabatic throughout the simulation. The velocities of the splat nodes touching the substrate are set to zero except the contact line node, where only the no-penetration condition is set. The usual axisymmetry condition is applied to all splat parameters on the Z-axis.

The conservation equation (1) - (3) are spatially discretized with a Galerkin FEM description. The weak formulation of the momentum equations reads:

$$\int_\Omega \phi_k D_\tau \vec{V} + \nabla\phi_k \cdot \overline{\underline{T}} + \phi_k \cdot \begin{pmatrix} \bar{\sigma}_{\theta\theta}/R \\ 1/Fr \end{pmatrix} d\Omega = \int_{\partial\Omega} \phi_k \cdot \left(\vec{n}^S \cdot \overline{\underline{T}}^S\right) d\Gamma \tag{7}$$

For elements at the free surface, the projection of the stress tensor $\overline{\underline{T}}$ onto the outer surface normal in Eq. (7) can be rewritten according to [10], Chap. VII:

$$\left(\vec{n}^S \cdot \overline{\underline{T}}^S\right) = -2\frac{\overline{H}}{We}\vec{n}^S + \nabla^S\left(\frac{1}{We}\right) \tag{8}$$

This formulation includes a variable surface tension, since a variable Weber number *We* and an additional surface tension gradient term is introduced. The upper script '*S*' denotes the evaluation at the surface and $\overline{H} = H/d_0$ is the dimensionless mean curvature defined as in [2].

2.2 Surface tension model

The surface tension of the liquid-vapor interface is considered to be a linear function of temperature:

$$\gamma = \gamma_{ref} + \left(d_T\gamma\right)_{ref}\left(T - T_{ref}\right) \tag{9}$$

The Weber number *We* in Eq. (8) has to be defined locally. With Eq. (9) one finds:

$$\frac{1}{We} = \frac{\gamma}{\rho d_0 v_0^2} = \frac{1}{We_{ref}} + \frac{Ma}{Re_0}\left(\Theta - \Theta_{ref}\right) \tag{10}$$

Hereby, the Marangoni number *Ma* and the dimensionless temperature Θ are introduced:

$$Ma = \frac{Re_0}{We_0}\frac{\left(d_T\gamma\right)_{ref}\left(T_{1,0} - T_{2,0}\right)}{\gamma_0} \tag{11}$$

With this, Eq. (8) changes to:

$$\left(\vec{n}^S \cdot \overline{\underline{T}}^S\right) = -2\frac{\overline{H}}{We}\vec{n}^S + \frac{Ma}{Re_0}\nabla^S\Theta \tag{12}$$

The thermophysical properties of solder used in this study and shown in Table 1 are carefully chosen and attuned to several literature sources [11] [12].

2.3 Wetting model

Spontaneous wetting or de-wetting occurs when the Gibbs free energy of the system can be altered. The spreading of liquids over a solid surface as a rolling motion, [13], implies a contact angle of 180 degree in case of a no-slip condition at the contact line and a zero-thickness interface to fulfill all hydrodynamic conditions [5]. If at all, this maximum value of the contact angle is primarily observed during the initial stage of the droplet deposition stage where the dynamic pressure in the contact region deforms the free surface accordingly. At later stages, the wetting is further driven due to the uncompensated Young force at the contact line [14], with wetting angles typically far below the maximum value mentioned above. As shown by [3], a conventional hydrodynamic model requires the allowance of slip at the contact line to avoid a stress singularity and an additional wetting model to capture realistic wetting angles.

The slip wetting model proposed in the present work is in principle a combination of the Navier-slip condition and a slip velocity proportional to the local gradient of the thermodynamic potential, represented by the uncompensated Young force at the contact line:

$$\left(\vec{n}^{\,S} \cdot \underline{\underline{T}}^{S} \cdot \vec{e}_R \right)_{CL-Segment} = \frac{1}{2 \cdot \pi \cdot R_{CL}} \left(\frac{1}{We_{sv}} - \frac{1}{We_{sl}} - \frac{cos(\theta)}{We} \right) \tag{13}$$

Here, We_{sv}, We_{sl} and We are the Weber number of the solid-vapor, solid-liquid and the liquid-vapor interface respectively, whereas the latter is defined as in Eq. (10). $\vec{e}_R$ is the radial unity vector, R_{CL} is the current radius of the contact line and θ is the dynamic contact angle. Equation (13) defines implicitly a radial gradient in surface tension at the contact line, which extends a finite length and has to be compensated by fluid stresses. If the fluid at the solid-liquid interface is considered to have been initially part of the liquid-vapor surface, this assumption coincides with the statement that the surface tension relaxation proceeds on a macroscopic length scale and not in a singular point [15].

Fowkes proposed an equation to estimate the interfacial energy through dispersion interaction at a contact line [16]:

$$\gamma_{sl} = \gamma_{sv} + \gamma - 2 \cdot \left(\gamma_{sv}^{d} \cdot \gamma^{d} \right)^{1/2} \tag{14}$$

γ_{sl}, γ_{sv} and γ are the specific surface energies of the solid-liquid, solid-vapor and the liquid-vapor interface respectively. The more general approach in [17] multiplied the dispersive adhesion work term in Eq. (14) with an empirical parameter ϕ_G, which can be adjusted to consider polar interaction to some extent as well [18]. The parameter ϕ_G is according to [19] approximately equal to 0.947 for solid copper. Using Eq. (14) and the Good-parameter ϕ_G, Eq. (13) becomes:

$$\left(\vec{n} \cdot \underline{\underline{T}} \cdot \vec{e}_R \right)_{CL-Segment} = \frac{1}{2 \cdot \pi \cdot R_{CL}} \left(2 \cdot \phi_G \cdot \left(\frac{1}{We_{sv} \cdot We} \right)^{1/2} - \frac{1 + cos(\theta)}{We} \right) \tag{15}$$

The surface energy of the solid-vapor interface is taken from [19] as 1710 mJ/m^2, which provides a Weber number of $We_{sv} = 0.8651$. With an average liquid-vapor Weber number of $We = 3.0$ it can be shown that the right side of Eq. (15) is always larger than zero, even for a contact angle of zero degree. This means indefinite, complete wetting and consequently no equilibrium contact angle should be attained in the case of isothermal spreading [20].

Equation (15) is applied to the contact line node and to its first neighbor on the solid-liquid interface. The cosine-term in Eq. (15) is already considered if Eq. (12) is applied to the contact line as well and is therefore dropped in the implementation.

2.4 Numerical solution procedure

The solution procedure was extensively outlined in earlier works [2]. Only the previously used commercial meshing tool Hypermesh® was replaced by the public-domain software Mesh2D for the simulations using the proposed wetting condition. The tool is capable to mesh adaptively according to the local gradient of a freely defined scalar, in this case the pressure.

The simulations using a fixed grid size were employing about 6500 elements and took 28h to complete 50'000 time steps, whereas the adaptive grid used about 9100 elements and 35h CPU time (1GHz, Pentium III). The accuracy in spreading prediction was increased by locally refining the grid at the contact line area for the latter cases. A number of simulations were performed in order to ensure mass and energy conservation. For the mesh density and time step utilized, both mass and energy were conserved within a final error of less than 1% compared to the initial values. Furthermore, it was verified that mesh and time step independent solutions were obtained.

2.5 Parameter variations

In order to investigate the effects of the temperature dependence of surface tension and of the proposed wetting force on the spreading, the transient behavior as well as on the end shape of the droplet, simulations were performed utilizing different values of droplet superheat. The initial droplet temperature was changed from 200°C to 500°C in steps of 100K. The droplet impact velocity was kept constant at 1.5 m/s and the initial droplet diameter also remained unchanged at the typical value for solder jetting of 80 μm. However, due to the change of the initial droplet temperature, the initial Weber and Marangoni number changed from case to case. The influence of the changing viscosity with increasing droplet superheat was partly considered by adjusting the initial Reynolds number appropriately. Table 2 summarizes the simulations performed and the corresponding parameter values (NSC – Navier-Slip Condition, PWC – Proposed Wetting Condition).

3 Results and discussion

Considering the droplet post-solidification shapes in Fig. 1, every figure compares the end shapes of two cases at a specific droplet superheat: The first involves the Marangoni effect and uses the Navier-slip condition (dotted line), whereas the second case employs the Marangoni effect as well as the proposed wetting condition (solid line). For the cases applying the Navier-slip condition, spreading is reduced monotonically with increasing absolute Marangoni number by about 18%. The reduced spreading with increasing absolute Marangoni number is a counter-intuitive result. Equation (12) suggests that the direction of the Marangoni force points towards the substrate, since the Marangoni number is negative and the temperature gradient is positive. One would expect a surface flow in the direction of the contact line, thereby accumulating mass and actually enhancing the spreading. In fact the opposite is observed, spreading is reduced. This was previously shown to be the effect of the emergence of negative vorticity in the contact region [2].

If the Navier-slip model is replaced by the proposed wetting condition, spreading enlarges about 10% with increasing absolute Marangoni number, Fig. 1. Recognizing that the wetting force expressed in Eq. (15) is always directed in positive radial direction due to the large specific surface energy of the solid-vapor interface, the explanation is as follows:

Table 1 Thermophysical Properties of Sn63Pb @ 260°C

		Liquid	Solid
Density ρ	[kg/m^3]	8218	8240
Viscosity μ_{ref}	[mPas]	2.237	-
Surf. Tens. γ_{ref}	[mN/m]	498.53	-
Surf. Tens. Slope $(d_T\gamma)_{ref}$	[mN/mK]	-0.214	-
Heat Capacity c_p	[J/kgK]	238	176
Thermal Conductivity k	[W/mK]	25	48
Latent Heat of Fusion L	[kJ/kg]	4.2	4.2
Melting Point T_m	[°C]	183	183

Table 2 Parameter Variations in Simulations

Run	Slip	$T_{1,0}$	Re_{ref}	We_{ref}	Ma_{ref}
A1	NSC	200°C	361	2.89	-9
A2	PWC	200°C	361	2.89	-9
B1	NSC	300°C	492	3.02	-19
B2	PWC	300°C	492	3.02	-19
C1	NSC	400°C	610	3.16	-33
C2	PWC	400°C	610	3.16	-33
D1	NSC	500°C	716	3.31	-49
D2	PWC	500°C	716	3.31	-49

The increasing droplet superheat delays the freezing at the contact line, providing therefore more time to accelerate the contact line outward by the wetting force and to increase the spreading.

The question arises whether the previously observed reduction in spreading due to the Marangoni effect is a pure artifact of the Navier-slip condition used. To clarify this, simulations were conducted employing the proposed wetting condition but excluding the Marangoni effect. Spreading increased in these cases up to 20% with increasing absolute Marangoni number (not shown here). This suggests that indeed the Marangoni effect reduces the spreading due to the emergence of negative vorticity in the contact region as stated before. In brief, without Marangoni effect there exist two counter-rotating vorticity regions at the contact line, a negative one close to the liquid-solid interface and a positive one close to the vapor-liquid interface. These two vorticity regions are assumed to drive the initial spreading. The positive vorticity region is reduced through the Marangoni effect since the Marangoni force opposes the direction of rotation. As a result, the spreading is reduced. However, the strong reduction in spreading due to the Marangoni effect as in the cases employing the Navier-slip condition is not observed and seems to be partly an artifact of the Navier-slip condition. The Navier-slip condition leads hereby to wetting velocities between -0.48 m/s and 3.9 m/s, whereas the contact line speeds obtained with the proposed wetting condition reside within -0.11 m/s and 3 m/s. The maximum absolute de-wetting velocity is therefore four times larger with the Navier-slip condition than with the proposed wetting condition and supports the observation that the Navier-slip condition overestimates the receding slip velocity. This can be reasoned with the mathematical formulation of the Navier-Slip condition [5]:

$$\left(\vec{n}\cdot\overline{\overline{T}}\cdot\vec{t}\right)_{CL-Segment}=\frac{1}{\varepsilon}\left(\vec{V}\cdot\vec{t}\right)_{CL} \tag{16}$$

The normal vector in this case is equal to $(0,-1)^T$ and the tangential vector is the radial unity vector $\vec{e}_R$. This implies that the projection of the stress tensor onto the contact line segment is equal to the stress tensor component $\bar{\sigma}_{RZ}$ stated as in Eq. (5) multiplied with -1. Note that the Navier-slip length ε does not represent an actual physical length and is assumed to be of the order $O(Re\cdot 10^3)$ within this study. [21] showed that spreading is almost invariant for variations of $O(10^5)$ in the slip lengths. The axial velocity V is zero along the solid-liquid interface (no-penetration condition) and Eq. (16) changes to:

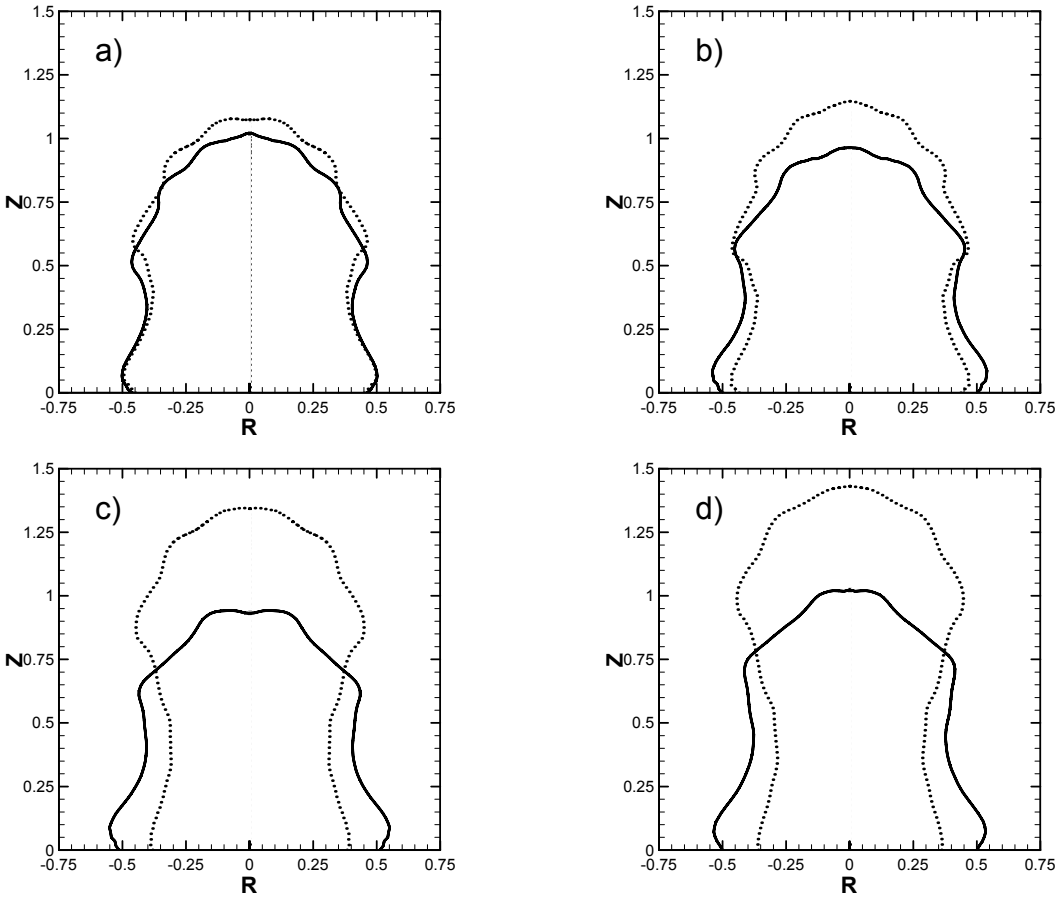

Fig. 1 a) – b) Change of spreading and solidified droplet shape with increasing superheat, droplet superheat 200°C - 500ºC, variation in steps of 100K
Dotted line: Variable surface tension and Navier-slip condition
Solid line: Variable surface tension and proposed wetting condition

$$U_{CL,NSC} = -\frac{\varepsilon}{Re}\left(\partial_Z U\right)_{CL} = \frac{\varepsilon}{Re}\omega_{CL} \tag{17}$$

ω_{CL} is the dimensionless vorticity at the contact line segment defined as:

$$\omega_{CL} = \left(\partial_R V - \partial_Z U\right)_{CL} = -\left(\partial_Z U\right)_{CL} \tag{18}$$

Applying similar derivations to Eq. (15), an estimation for the vorticity at the contact line in case of the proposed wetting condition can be obtained:

$$\omega_{CL,PWC} = \frac{Re}{2\cdot\pi\cdot R_{CL}}\left(2\cdot\phi_G\cdot\left(\frac{1}{We_{vs}\cdot We}\right)^{1/2} - \frac{1+cos\left(\theta\right)}{We}\right) \tag{19}$$

Equation (17) points out that as soon as the vorticity in the contact region is negative, the Navier-slip velocity $U_{CL,NSC}$ is negative as well and the droplet recedes. The proposed wetting condition imposes instead a positive vorticity throughout the impact at the contact region due to the large solid-vapor Weber number used. It should additionally be mentioned, that the Navier-slip condition completely disregards wetting effects.

Both slip models inherit large dynamic wetting angles between 140 and 180 degree, which are primarily created by the dynamic pressure of the impact. This affirms the statement of [1] that wetting effects are indeed negligible in the parametric domain of solder jetting.

4 Conclusion

The numerical investigation presented herein studied the effect of thermocapillarity on the surface deposition process of picoliter size solder droplets in conjunction with two different slip models at the contact line. The conventional Navier-slip condition and a wetting condition based on the uncompensated Young force at the contact line were employed. The previously stated reduction of spreading with increasing absolute Marangoni number obtained with the Navier-slip condition could not be found with the proposed wetting condition. However, it was shown that the Marangoni force hindered spreading also in the latter case, verifying the presumed mechanism of a vorticity reduction in the contact region. The over-prediction in droplet receding in case of the Navier-slip condition was accounted to the theoretical connection between slip velocity and vorticity imposed by this condition at the contact line. The proposed wetting condition implies instead positive vorticity at the contact line throughout the deposition. Further theoretical and experimental investigations needs to be done to verify the proposed wetting condition.

Acknowledgement

Mesh2D was developed by Francis X. Giraldo at Naval Research Lab., Monterey, U.S.A.

5 References

[1] Attinger, D. Zhao, Z. *et al.*, 2000, Journal of Heat Transfer-Transactions of the Asme, **122**, 544-556
[2] Dietzel, M. Haferl, S. *et al.*, 2003, Journal of Heat Transfer-Transactions of the Asme, **125**, 365-376
[3] Dussan, E. B. Davis, S. H., 1974, Journal of Fluid Mechanics, **65**, 71-&
[4] DeConinck, J. Voue, M., 1997, Interface Science, **5**, 141-145
[5] Baer, T. A. Cairncross, R. A. *et al.*, 2000, International Journal for Numerical Methods in Fluids, **33**, 405-427
[6] Hoffman, R. L., 1975, Journal of Colloid and Interface Science, **50**, 228-241
[7] Fukai, J. Shiiba, Y. *et al.*, 1995, Physics of Fluids, **7**, 236-247
[8] Pismen, L. M. Rubinstein, B. Y., 2001, Langmuir, **17**, 5265-5270
[9] Haferl, S. Butty, V. *et al.*, 2001, International Journal of Heat and Mass Transfer, **44**, 3513-3528
[10] Landau, L. D. Lifshitz, E. M., 1959, Fluid Mechanics, Pergamon Press
[11] Keene, B. J., 1993, International Materials Reviews, **38**, 157-192
[12] Carroll, M. A. Warwick, M. E., 1987, Materials Science and Technology, **3**, 1040-1045
[13] Shikhmurzaev, Y. D., 1994, Fluid Dynamics Research, **13**, 45-64
[14] Schiaffino, S. Sonin, A. A., 1997, Physics of Fluids, **9**, 3172-3187
[15] Blake, T. D. Bracke, M. *et al.*, 1999, Physics of Fluids, **11**, 1995-2007
[16] Fowkes, F. M., 1962, Journal of Physical Chemistry, **66**, 382-&
[17] Girifalco, L. A. Good, R. J., 1957, Journal of Physical Chemistry, **61**, 904-909
[18] Chibowski, E. Ontiveros-Ortega, A. *et al.*, 2002, Journal of Adhesion Science and Technology, **16**, 1367-1404
[19] Hara, S. Hanao, M. *et al.*, 1993, Journal of the Japan Institute of Metals, **57**, 164-169
[20] Yang, J. X. Koplik, J. *et al.*, 1992, Physical Review A, **46**, 7738-7749
[21] Haferl, S. E. L., 2001, Ph.D. thesis, Swiss Federal Institute of Technology